Potential room-temperature multiferroicity in cupric oxide under high pressure

William Lafargue-Dit-Hauret,[1,*] Daniel Braithwaite,[2] Andrew D. Huxley,[3] Tsuyoshi Kimura,[4] Andres Saúl,[5] and Xavier Rocquefelte[1,†]

[1]*Univ Rennes, CNRS, ISCR (Institut des Sciences Chimiques de Rennes) UMR 6226, F-35000 Rennes, France*
[2]*Univ. Grenoble Alpes, Grenoble INP, CEA, IRIG-Pheliqs, F-38000 Grenoble, France*
[3]*Centre for Science at Extreme Conditions and SUPA, School of Physics and Astronomy, University of Edinburgh, Edinburgh, EH9 3JZ, United Kingdom*
[4]*Department of Advanced Materials Science, University of Tokyo, Kashiwa, Chiba 277-8561, Japan*
[5]*Aix Marseille Univ, CNRS, CINaM UMR 7325, Campus de Luminy Case 913, 13288 Marseille, France*

(Received 11 January 2021; revised 11 May 2021; accepted 1 June 2021; published 21 June 2021)

CuO, known to be multiferroic (MF) from $T_L = 213$ K to $T_N = 230$ K at ambient pressure, has been the subject of debates about its ability to exhibit multiferroicity at room temperature (RT) under high hydrostatic pressure. Here we address this question based on theoretical and experimental investigations. The influence of hydrostatic pressure on T_L and T_N has been estimated from *ab initio* calculations combined with classical Monte-Carlo simulations and a quasi-1D antiferromagnetic analytical model. From the experimental side, electric permittivity anomalies related to ferroelectric transitions have been followed with dielectric measurements on single crystals up to 6.1 GPa. We show that the temperature T_N below which the MF state forms increases with pressure linearly to higher pressure that hitherto supposed, and indeed based on our calculations, should exceed RT above about 20 GPa.

DOI: 10.1103/PhysRevB.103.214432

I. INTRODUCTION

Multiferroic (MF) materials are usually associated with compounds that simultaneously exhibit magnetism and ferroelectricity. The coexistence of both ferroic orders has attracted considerable attention from industry and academic researchers for several decades [1–4]. Indeed, the development of magnetoelectric materials operating at room temperatures (RT) constitutes the holy grail in this field. They could play key roles in magnetic field sensors or memory devices and also advance in the fundamental understanding of the coupling between the two degrees of freedom. In such compounds, the electric polarization can be controlled through the application of a magnetic field, and an electric field can be used to orientate the macroscopic magnetization. Beyond the difficulty of finding systems in which both properties are coupled at sufficiently high temperatures, some industrial constraints must also be fulfilled: Miniaturization, high power efficiency, biocompatibility, low cost, etc.

Thirteen years ago, experimental investigations demonstrated that cupric oxide CuO exhibits magnetoelectric properties [5]. The ferroelectricity appears to emerge from the incommensurate noncollinear magnetic order (hereafter labeled AF_2) existing between the lock-in temperature T_L and the Néel temperature T_N located at 213 and 230 K, respectively. This incommensurate magnetic phase is characterized by a propagation vector $\boldsymbol{q} = (0.506, 0, -0.483)$ [6]. Below T_L, CuO shows a commensurate collinear antiferromagnetic (AFM) order (hereafter labeled AF_1) with all magnetic moments oriented along the crystallographic $\boldsymbol{b}$ axis. The anomalously high Néel temperature for a cuprate system and the significant electric polarization ($\sim 100\ \mu\mathrm{C\ m^{-2}}$ [7]) make this compound a promising candidate for high-temperature MF applications. However, it is limited by the small temperature range over which MF is found (i.e., only 17 K) that is still far from RT. Experimental studies have demonstrated that the application of a hydrostatic pressure below 2 GPa enlarges the MF stability domain by decreasing T_L and increasing T_N [8,9]. Based on the combination of density functional theory (DFT) and effective models (analytical and Monte Carlo simulations), multiferroicity at RT has been predicted to appear under an applied pressure of about 20–40 GPa [10]. In 2016, Jana *et al.* reported an experimental investigation which might suggest that CuO exhibits a RT ferroelectric polarization at a pressure of only 4.4 GPa [11]. In this study, polycrystalline samples were used without pressure transmitting medium leading to unavoidable nonhydrostatic pressure effects and inhomogeneities during the compression of the sample. In contrast, based on neutron and XRD analyzes performed on single crystals, Kozlenko *et al.* claimed that the upper limit of T_N would be 260 K at 38 GPa [12].

The aim of this paper is to discuss the possibility of RT multiferroicity in CuO through a combined theoretical and experimental investigation. Briefly, we calculated effective magnetic interactions and estimated the transition temperatures using powder experimental atomic structures obtained under hydrostatic pressures ranging from 0 to 38 GPa [12]. Experimentally, we present electric permittivity

*william.lafargue-dit-hauret@univ-pau.fr
†xavier.rocquefelte@univ-rennes1.fr

measurements as a function of temperature and pressure up to 6.1 GPa. The experiments show a continuous widening of the MF stability domain, which coupled with the theoretical calculations, allow to extrapolate the existence of a MF phase at RT when the pressure approaches 20 GPa.

II. METHODS

A. Crystal structure

CuO crystallizes within a $C2/c$ monoclinic phase defined by $a = 4.695$ Å, $b = 3.436$ Å, $c = 5.147$ Å, and $\beta = 99.46^\circ$ at zero pressure [12]. Cu atoms are located at the center of oxygen square planar environments. These entities, also called *plaquettes*, originate from an octahedral environment which undergoes a Jahn-Teller distortion. The three-dimensional (3D) atomic structure of CuO can be viewed as based on edge-sharing ribbons which are linked together through corners of CuO_4. It should be noticed that the related lattice parameters vary nonlinearly and anisotropically with pressure and temperature [13–16].

B. Computational details

1. First-principles calculations

DFT simulations have been carried out using the full-potential LAPW method as implemented within the Wien2k package [17]. The exchange-correlation term was set using the PBE0 on-site hybrid functional [18], which allows to treat a given set of strongly correlated electrons, namely $3d$-Cu orbitals. The muffin-tin radii were set to 1.94 and 1.67 a_0 for copper and oxygen atoms, respectively. The basis function expansion was set by the parameter $RK_{\max} = 7$. Calculations have been performed on the experimental structures provided in Ref. [12]. We investigated the electronic properties of the 8 formula unit magnetic cell [19] defined by $\boldsymbol{a_m} = \boldsymbol{a}$-$\boldsymbol{c}$, $\boldsymbol{b_m} = \boldsymbol{b}$, and $\boldsymbol{c_m} = \boldsymbol{a}$+$\boldsymbol{c}$, where $\boldsymbol{a}$, $\boldsymbol{b}$, and $\boldsymbol{c}$ are the lattice parameters of the $C2/c$ unit cell. Integrations in the first Brillouin zone were performed with a $5 \times 11 \times 6$ Monkhorst-Pack k-mesh. For magnetic interactions, we estimated the J_{ij} magnetic exchange couplings by fitting 13 nonequivalent magnetic configurations with an Ising model [20–25]. The following convention has been considered for J_{ij} couplings: A positive sign corresponds to an AFM character, while a negative sign corresponds to a ferromagnetic (FM) interaction. We calculated the magnetocrystalline anisotropy (MCA) by including the spin-orbit coupling (SOC) as a second-order correction to the total energy.

2. Bloch spin states

The commensurability of the magnetic ground state, dictated by magnetic interactions, has been investigated by studying the dispersion of spin states [26]. The examination of the first-ordered state depending on the wave-vector $\boldsymbol{k}$ and isotropic exchange couplings J_{ij} was done by solving the eigenvalue problem:

$$\xi(\boldsymbol{k}, J_{ij})\sigma(\boldsymbol{k}, J_{ij}) = \lambda(\boldsymbol{k}, J_{ij})\sigma(\boldsymbol{k}, J_{ij}), \tag{1}$$

where σ is the spin configuration, λ is the energy of the branch, and ξ is the Fourier transform of the exchange integral matrix expressed as:

$$\xi(\boldsymbol{k}, J_{ij}) = \sum_m J_{ij}(\boldsymbol{R}_m)e^{-2\pi i \boldsymbol{k}\boldsymbol{R}_m}, \tag{2}$$

where $\boldsymbol{R}_m$ is the lattice vector separating spins i and j.

3. Classical Monte Carlo (CMC) simulations

The pressure vs temperature MF phase diagram was theoretically investigated by CMC simulations parametrized by an effective magnetic model expressed as:

$$H_{\text{model}} = H_H + H_{UA} + H_{DM} + H_{MA}, \tag{3}$$

where H_H is the Heisenberg term, H_{UA} is an uniaxial anisotropy parameter, H_{DM} is the Dzyaloshinskii-Moriya coupling, and H_{MA} is a multiaxial term. Details on the physical meaning and the construction of each term can be found in Ref. [10]. For each pressure, the magnetic interactions J_{ij} and MCA determined at 0 K within DFT were injected into the magnetic model. CMC calculations were done on a supercell made of 12^3 spins. Both thermalization and equilibration processes were performed on 10^6 CMC steps. MF phase transitions were extracted by following the spin current $\boldsymbol{P} \propto \langle \boldsymbol{e_{ij}} \times (\boldsymbol{S_i} \times \boldsymbol{S_j}) \rangle$, which relates the electronic contribution of the electric polarization $\boldsymbol{P}$ to the perpendicularly oriented magnetic moments $\boldsymbol{S_i}$ and $\boldsymbol{S_j}$ connected by the unit vector $\boldsymbol{e_{ij}}$ [27].

4. Quasi-1D magnetic model

Several experimental studies have concluded that CuO can be described as a quasi-1D antiferromagnet [28–31] with the Néel temperature T_N based on the random-phase approximation model of a quasi-1D AFM Heisenberg cubic lattice [32]:

$$J' = \frac{T_N}{4c\sqrt{\ln(\alpha J/T_N) + 0.5\ln[\ln(\alpha J/T_N)]}}, \tag{4}$$

where $\alpha = 2.6$ and $c = 0.233$ are numerical parameters, J' is an effective interchain coupling, and J is the intrachain coupling.

In 2013 [10], we used this model to describe the evolution of T_N with pressure. We showed that two solutions lead to similar results: (1) Adjusting c to 0.284 and keeping α equal to 2.6, and (2) adjusting α to 8.4 and keeping c equal to 0.233. In 2017, Kozlenko *et al.* [12], reconsidered our proposition, adjusting both c and α values to $c = 0.274$ and $\alpha = 1.5$. In addition, they considered empirical J_{ij} values based on the knowledge of superexchange angles.

As in our previous investigation [10], our calculations are based on the J_{ij} values obtained from DFT, taking into account their pressure dependence. We define $J = J_z$ and $J' = (J_{2a} - J_x)/2$ to coincide with the expression of the collinear magnetic ground-state energy defined as $E_{GS} = J_z - J_x + J_{2a}$. To adjust c and α values, we have considered not only the T_N value at 0 GPa but also the T_N value at 5 GPa, leading to $c = 0.237$ and $\alpha = 3.474$.

C. Experimental details

Dielectric measurements were carried out in a diamond anvil cell (DAC). The technique is described in detail

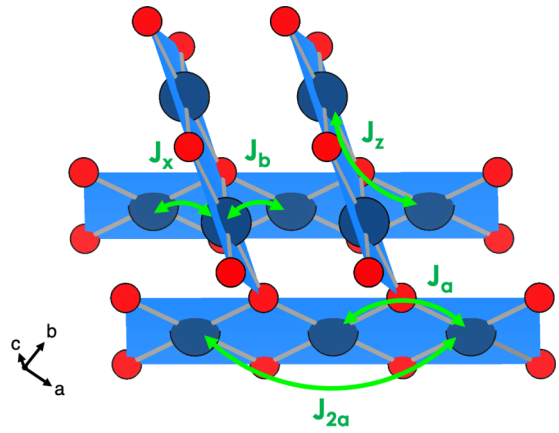

FIG. 1. Magnetic exchange couplings are considered in this study. The different interactions are highlighted by green arrows. Blue and red spheres indicate copper and oxygen atoms, respectively. Square planar environments are represented in blue.

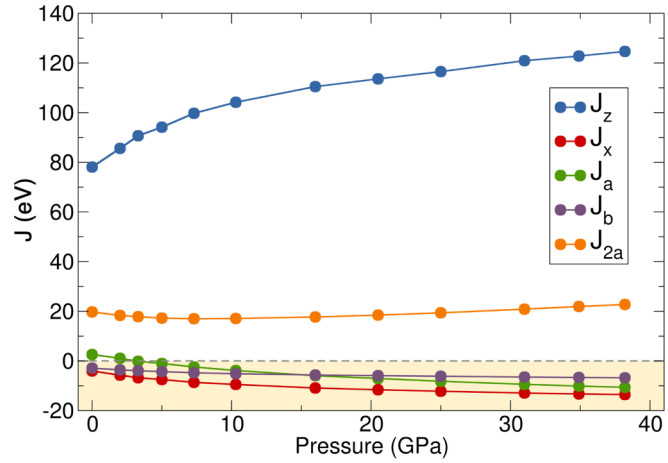

FIG. 2. Magnetic exchange interactions vs hydrostatic pressure. Positive and negative signs correspond to AFM and FM interactions, respectively.

elsewhere [33]. A single crystal of CuO was cleaved perpendicular to the b axis and polished to a thickness of about 40 μm. Pieces of size approximately 200 × 200 μm suitable for the DAC were then cleaved from this piece. A 10-μm gold wire was attached to each side of the sample with silver epoxy, which was spread to almost cover the whole surface. The sample wires were connected to two co-ax wires. The cell was loaded with liquid argon as the hydrostatic pressure medium, and the pressure was measured *in situ* using the ruby fluorescence technique. The capacitance of the sample, proportional to its dielectric constant, was measured with a capacitance bridge at 1 kHz (Andeen-Hagerling AH 2550A). The DAC was placed in a Gifford-McMahon cryocooler where the temperature could be swept from 300 K to about 20 K.

III. RESULTS AND DISCUSSIONS

A. J_{ij} couplings

In the last few years, many investigations have reported theoretical and experimental evaluations of the effective exchange interactions J_{ij} (see Ref. [34] for a summary). It should be noted that estimates for J_{ij} vary strongly depending on the effective Hamiltonian used for the experimental fit or the theoretical mapping.

The first step of all our calculations was to estimate the J_{ij} exchange couplings and the magnetocrystalline anisotropy (MCA). For this purpose, we used a similar procedure than the one considered in Ref. [10]. The difference is that instead of using theoretical atomic structures relaxed under a hydrostatic pressure varying from 0 to 200 GPa [10], we used the experimental structures extracted from Ref. [12] for pressure values going from 0 to 38 GPa. Here, five magnetic exchange interactions have been considered, depicted in Fig. 1. As shown in Fig. 2, their pressure dependence is very similar to the evolution under pressure predicted for the theoretically calculated structures [10].

In short, five J_{ij} exchange interactions (where $i \neq j$) are sufficient to describe the magnetic properties of CuO [10,35,36]. Among them, two are significantly larger, i.e., corner sharing J_z and next nearest-neighbor intraribbon J_{2a} with values of about 80 and 20 meV at 0 GPa, respectively. The three others (J_x, J_a and J_b) are smaller. Under pressure, J_z rises from 78.1 meV (0 GPa) to 124.6 meV (38 GPa). The second most important interaction corresponds to J_{2a}, which remains roughly unchanged with the pressure varying slightly from 19.7 (0 GPa) to 22.7 meV (38 GPa). Regarding the nearest-neighbor intraribbon coupling J_a, the increase of the hydrostatic pressure changes its character from AFM to FM above ∼3 GPa. The value of this coupling ranges from 2.6 meV (0 GPa) to −10.6 meV (38 GPa). The other two interribbon interactions J_x and J_b become more and more FM with pressure, reaching −13.6 and −6.8 meV at 38 GPa, respectively.

To our knowledge, the experimental pressure dependence of the J_{ij} exchange interactions has not been reported, so far. We will thus compare our calculations with the ambient pressure neutron-scattering experimental data [34], as summarized in Table I. The authors applied constraints to simplify their Hamiltonian, leading to differences with our Hamiltonian. In our case, we consider not only the Cu-Cu interatomic distances to define a magnetic exchange path but also the overlap of the magnetic orbitals (bond or dihedral angles). As a consequence, a correction of a factor of 2 must be applied to J_{2a} and J_a deduced from neutron scattering to compare with our results, leading to 6.34 and ±5.0 meV, respectively. The agreement with DFT is good except for J_{2a} for which DFT gives a higher value (19.7 meV). J_{2a} corresponds to a super-superexchange interaction between two coplanar CuO_4

TABLE I. Magnetic exchange interactions (in meV) computed for the 0 GPa structure. The interatomic distances are given in Å, and the inelastic neutron values from Ref. [34] are also reported.

	J_z	J_x	J_a	J_b	J_{2a}
d^{0GPa}_{Cu-Cu}	3.757	3.186	2.909	3.095	5.819
This work	78.1	−4.0	2.6	−2.9	19.7
Exp. [34]	91.4(5)	−3.73(3)	±2.50(18)	±3.10(18)	3.17(3)

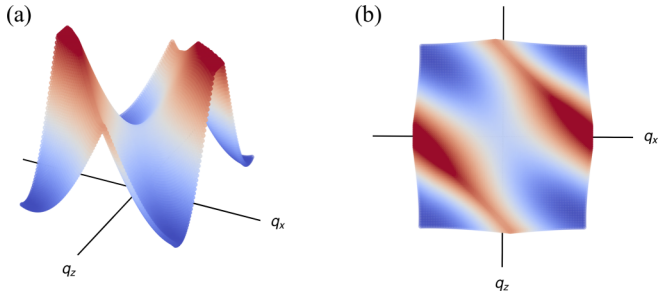

FIG. 3. (a) Diagonal and (b) top view of the dispersion of the magnetic ground state within the $(\boldsymbol{q_x}, \boldsymbol{q_z})$ plane at 0 GPa. The red color highlights highest energies, while dark blue regions evidence energy minima.

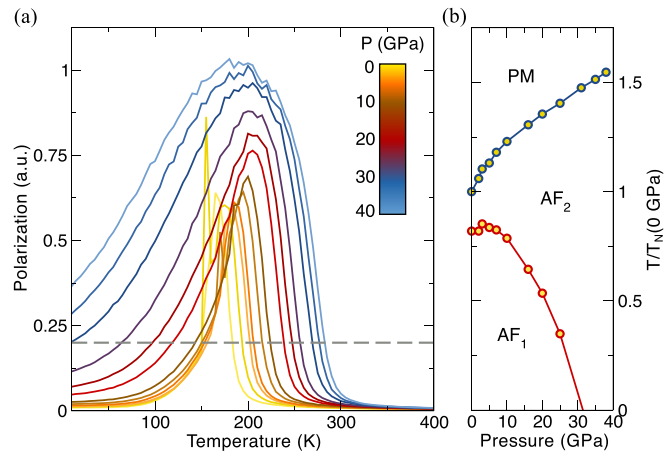

FIG. 4. CMC results. (a) Electric polarization vs temperature for different pressure values. The electric polarization was estimated by $\boldsymbol{P} \propto \langle \boldsymbol{e}_{ij} \times (\boldsymbol{S}_i \times \boldsymbol{S}_j) \rangle$. The gray dashed line is the reference arbitrarily chosen to estimate the MF phase transitions. (b) MF phase diagram. T_L and T_N variations are represented by red and blue lines, respectively, and normalized at the estimated CMC T_N value at 0 GPa.

plaquettes. As a consequence, the overlap between the magnetic orbitals, through the $2p$-O states, is optimal, and thus a large value is not counterintuitive. Interpreting this deviation is not straightforward. From the point of view of the neutron-scattering experiments, no clear evidence of a coupling of about 20 meV has been identified. Only one path in the reported magnetic dispersion probes the effect of J_{2a}, leading the authors to conclude that J_{2a} is necessary to reproduce the minimum in the dispersion at the X point, corresponding to $\boldsymbol{q} = (1, 1/2, 0)$. However, the effect of J_{2a} is strongest in the direction from $(1/2, 0, -1/2)$ to $(1, 1/2, -1/2)$, and the last point is not given in the reported data.

B. MCA

We estimated the MCA by including the SOC. We found that the intensity of MCA is weakly affected even under relatively high pressures (see Supplemental Material [37]). In addition, the easy magnetization axis is unchanged under pressure up to 38 GPa, the magnetic moments being still preferentially oriented along the [010] direction, in the lines of experimental observations at 0 GPa [6]. These results closely agree with our previous predictions [10]. One may notice that the intermediate magnetization axis, computed at ambient pressure, is found within the ac plane with an angle of 60° with respect to the $\boldsymbol{c}$ crystallographic axis. This prediction significantly differs from the experimental value of 28.8(8)° revealed by neutron measurements [38]. The understanding of this difference is the subject of ongoing collaborative works combining Torque magnetometry analysis and DFT calculations.

C. Incommensurate magnetic structure

Neutron scattering has shown that the low-temperature ground-state magnetic structure AF_1, with a propagation vector $\boldsymbol{q} = (0.5, 0, -0.5)$, is commensurate with the crystallographic cell, while the AF_2 magnetic structure is incommensurate at ambient pressure with $\boldsymbol{q} = (0.526, 0, -0.483)$ [6]. Based on the Freiser method [26], the knowledge of the magnetic exchange couplings allows us to estimate the total spin-exchange energy for a given propagation vector $\boldsymbol{q}$. Figure 3 depicts the Bloch spin states of minimal energy within the $(\boldsymbol{q_x}, \boldsymbol{q_z})$ plane for 0 GPa. As can be seen, the maxima are found close to the middle of the edges of the Brillouin zone $(\pm 0.5, 0)$ and $(0, \pm 0.5)$ and the minima close to the corners $(\pm 0.5, \pm 0.5)$. Such a situation implies the magnetic cell can only be described by a crystal supercell, which follows nicely the experimental observations [6].

We obtained $\boldsymbol{q} = (0.53, 0, -0.45)$ at 0 GPa, in good agreement with the AF_2 experimental propagation vector [6,38,39]. We have then used the Freiser approach to predict the evolution of the magnetic structure under pressure. At 38 GPa, we found $\boldsymbol{q} = (0.50, 0, -0.47)$, suggesting that the magnetic structure of CuO remains incommensurate up to roughly 40 GPa.

Finally, let us note that based on a similar analysis, Dai *et al.* [40] concluded that the incommensurability of the magnetic structure originates from the J_b interaction. By decomposing our Ising hamiltonian and estimating the impact of each contribution, we found that not only J_b but also J_a take part in this spin spiral behavior.

D. MF phase diagram

The theoretical estimation of the variation of the Néel temperature T_N with pressure has been obtained using two different approaches, i.e., by performing CMC simulations and by using an analytical model. Let's first discuss our results deduced from CMC calculations, which were performed using the effective magnetic model expressed in Eq. (3) with similar settings to Ref. [10]. More specifically, the Heisenberg term H_H aims to describe the long-range magnetic ordering through exchange interactions. The H_{UA} uniaxial contribution was used to stabilize the AF_1 phase at low temperature, while the H_{DM} noncollinear term allows incorporation of the Dzyaloshinskii-Moriya coupling to favor the AF_2 phase. Finally, the H_{MA} multiaxial part constrains the magnetic moments within the $(\boldsymbol{b}, \boldsymbol{c})$ plane. By following the evolution of the electric polarization for each pressure step [see Fig. 4(a)],

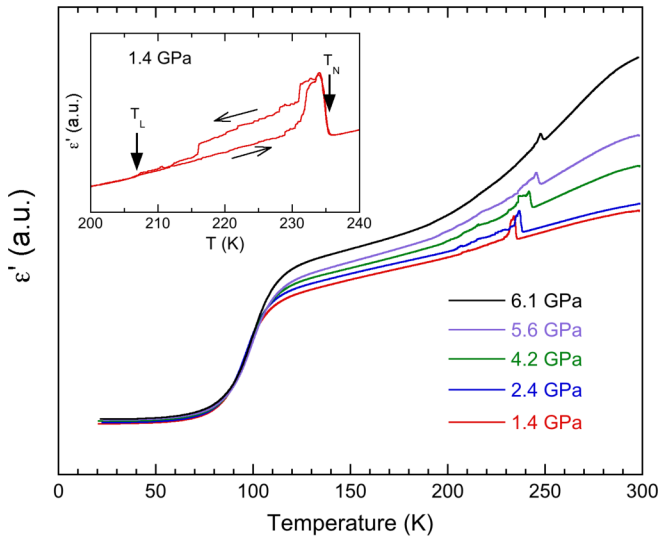

FIG. 5. Dielectric constant curves of single crystal CuO for $\boldsymbol{E}//\boldsymbol{b}$ from high-pressure capacitance measurements with increasing temperature. The inset shows the region of the two magnetic phase transitions for 1.4 GPa, indicated by the arrows. The upper transition (T_N) appears as a sharp step reproducible on warming and cooling. The lower transition (T_L) appears as a much smaller anomaly. The region between T_L and T_N shows marked hysteresis between the cooling and the warming cycles, with irreproducible behavior on cooling.

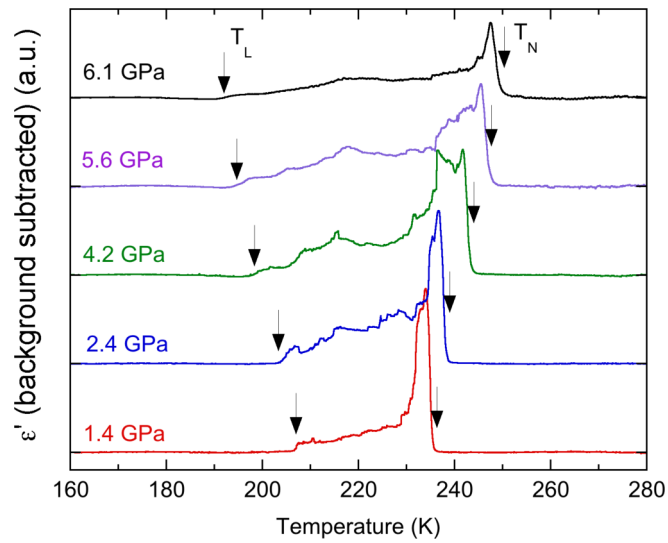

FIG. 6. Zoom of the dielectric constant curves shown in Fig. 5 after subtraction of an arbitrary polynomial background to reveal T_N and T_L transitions evidenced by arrows. Curves have been shifted for clarity.

the magnetic phase diagram has been evaluated and is presented in Fig. 4(b).

First, we found that the electric polarization induced by the noncollinear orientation of magnetic moments increases with pressure. Second, the MF stability domain expands, i.e., T_L decreases while T_N increases, with pressure. These results still agree with our previous predictions, which were based on theoretical structures. Here, we showed that using the experimental refined structures, CMC simulations predict a continuous increase of T_N without reaching a plateau as suggested by Kozlenko *et al.* [12].

E. Experimental dielectric measurements

In parallel, we measured the electric permittivity as a function of temperature up to 6.1 GPa. In Fig. 5, we show the dielectric constant curves for different pressures. A smooth but significant decrease of ε' below 100 K is present at all pressure steps. Such behavior has also been reported by Zheng *et al.* [41], attributed to a coupling between the magnetic and the vibrational degrees of freedom. At RT, ε' is found to increase monotonically with pressure, similar to the initial increase reported by Jana *et al.* [11]. However, we do not retrieve the sharp decrease of the dielectric constant that they observed at 4.4 GPa and assigned to the ferroelectric transition. Also, it is not clear why the transition would induce such a large drop of ε' as this is not the case at ambient pressure. From our data, the T_N transition is clearly observed at all pressures as a sharp step, which is reproducible between the cooling and the warming cycles. For temperatures ranging between T_N and T_L, the measurement shows hysteretic and nonreproducible behavior as shown in the inset. T_L can, however, be reliably detected as a small anomaly better seen in the warming curves. To reveal the two transitions, we show in Fig. 6 the previous curves after subtraction of a polynomial background and with an offset for the different pressures.

From our measurements, the experimental lower and upper limits of spin-spiral stability domain, i.e., T_L and T_N, are represented by red circles in Fig. 7. In addition, this figure shows the experimental data of Chatterji *et al.* [8] (open red diamonds) and our theoretical predictions. Two types of calculations are represented: (1) The CMC data, which have been shifted to fit the experimental T_N value at 0 GPa; (2) an analytical model suited for $S = 1/2$ quasi-1D Heisenberg antiferromagnets. First of all, the CMC data are not expected to provide quantitative results, but general trends. In contrast, the analytical model, if properly defined, should lead to quantitative results. Figure 7(a) shows a relatively good agreement between experiments and theory, confirming the increase (decrease) of T_N (T_L) with pressure and thus the stabilization of the spin-spiral magnetic phase, which exhibits multiferroicity. Our simulations suggest that T_N may reach RT at a pressure value of about 20 GPa, in agreement with our previous prediction.

A closer look at the data [Fig. 7(b)] shows evidence of some deviations in the CMC theoretical data compared to the experimental points, in particular for the evolution of T_L in the pressure range [0,2] GPa. It is probably due to the approximations made in the CMC model to describe the noncollinearity in AF_2 with the effective H_{DM} and H_{MA} terms. This trend would be improved by estimating such couplings with further noncollinear *ab initio* calculations, which is beyond the scope of this paper.

As shown in Fig. 7, this experimental study is consistent with previous experimental results obtained up to ∼2 GPa [8] and confirms our predictions of a continuous widening of the MF phase with pressure. In details, we find quasilinear variations of T_L and T_N over the studied pressure range, with

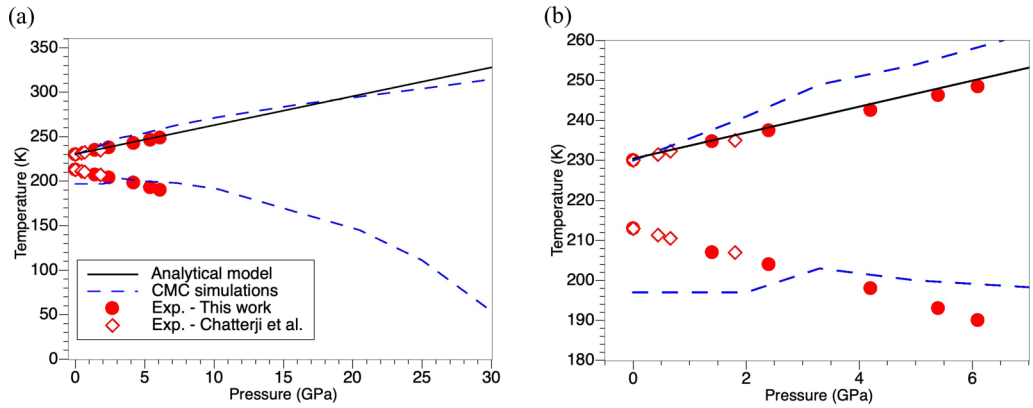

FIG. 7. (a) Temperature-pressure phase diagram of CuO. (a) Experimental values extracted from our dielectric measurements (red plain circles) and from Chatterji *et al.* [8] (red open diamonds). Our theoretical estimated values from CMC and the analytical expression [Eq. (4)] are represented by black lines and blue dashed lines, respectively. Our CMC simulations have been adjusted to fit the experimental Néel temperature at 0 GPa. (b) Zoom in the pressure range from 0 to 7 GPa to emphasize the experimental/theoretical deviations.

$(dT_L)/dP = -3.7$ K GPa^{-1} and $(dT_N)/dP = 3.0$ K GPa^{-1}. This strengthens our theoretical predictions on a significant increase of T_N for CuO under hydrostatic pressure without expected saturation as suggested by Kozlenko *et al.* [12]. Thus, these results support the hypothesis that MF properties can be observed at RT.

IV. CONCLUSION

We combined theoretical and experimental methods to follow the stability domain of the MF phase of CuO under hydrostatic pressure. From the theoretical side, we confirm our previous predictions using the refined atomic structures up to about 38 GPa in Ref. [12]. More specifically, T_L decreases while T_N increases under pressure. Experimental dielectric anomalies have been measured up to 6.1 GPa. We observed that T_L (T_N) linearly decreases (increases) with pressure, without detecting any saturation phenomenon. Together these results strongly support the possibility of RT multiferroicity in CuO under a pressure of about 20 GPa.

ACKNOWLEDGMENTS

The theoretical work was granted access to the HPC resources of TGCC/CINES/IDRIS under Allocation No. 2017-A0010907682 made by GENCI. W.L.-D.-H. and X.R. also acknowledge the CCIPL (Centre de Calcul Intensif des Pays de la Loire) for computing facilities, S. Kumar for helpful discussions, and M. Herak for fruitful discussions and comments on the manuscript. D.B., X.R., and A.S. acknowledge funding from the French National Research agency (ANR - Grant No. ANR-19-CE08-0013-02; HTHPCM Project). T.K. was supported by JSPS KAKENHI under Grants No. JP17H01143 and No. JP19H05823. D.B. and A.D.H. acknowledge support from EPSRC Grant No. EP/R013004/1.

[1] T. Kimura, Spiral magnets as magnetoelectrics, Annu. Rev. Mater. Res. **37**, 387 (2007).
[2] J. F. Scott, Room-temperature multiferroic magnetoelectrics, NPG Asia Mater. **5**, e72 (2013).
[3] S. Dong, J.-M. Liu, S.-W. Cheong, and Z. Ren, Multiferroic materials and magnetoelectric physics: Symmetry, entanglement, excitation, and topology, Adv. Phys. **64**, 519 (2015).
[4] M. Fiebig, T. Lottermoser, D. Meier, and M. Trassin, The evolution of multiferroics, Nat. Rev. Mater. **1**, 16046 (2016).
[5] T. Kimura, Y. Sekio, H. Nakamura, T. Siegrist, and A. P. Ramirez, Cupric oxide as an induced-multiferroic with high-T_c, Nat. Mater. **7**, 291 (2008),.
[6] J. B. Forsyth, P. J. Brown, and B. M. Wanklyn, Magnetism in cupric oxide, J. Phys. C: Solid State Phys. **21**, 2917 (1988).
[7] P. Babkevich, A. Poole, R. D. Johnson, B. Roessli, D. Prabhakaran, and A. T. Boothroyd, Electric field control of chiral magnetic domains in the high-temperature multiferroic CuO, Phys. Rev. B **85**, 134428 (2012).
[8] T. Chatterji, P. J. Brown, and J. B. Forsyth, High pressure neutron diffraction investigation of CuO, J. Phys.: Condens. Matter **17**, S3057 (2005).
[9] M. Ohashi, A. Tashiro, G. Oomi, E. Maeda, and X.-G. Zheng, Effect of pressure on the magnetic phase transition in cupric oxide, Phys. Rev. B **73**, 134421 (2006).
[10] X. Rocquefelte, K. Schwarz, P. Blaha, S. Kumar, and J. van den Brink, Room-temperature spin-spiral multiferroicity in high-pressure cupric oxide, Nat. Commun. **4**, 2511 (2013).
[11] R. Jana, P. Saha, V. Pareek, A. Basu, S. Kapri, S. Bhattacharyya, and G. D. Mukherjee, High pressure experimental studies on CuO: indication of Re-entrant multiferroicity at room temperature, Sci. Rep. **6**, 31610 (2016).
[12] D. P. Kozlenko, K. Drużbicki, S. E. Kichanov, E. V. Lukin, H.-P. Liermann, K. V. Glazyrin, and B. N. Savenko, Anomalous lattice compression and magnetic ordering in CuO at high pressures: A structural study and first-principles calculations, Phys. Rev. B **95**, 054115 (2017).

[13] M. Malinowski, S. Åsbrink, and A. Kvick, A high-pressure single-crystal X-ray diffraction study of copper oxide using synchrotron radiation, High Press. Res. **4**, 429 (1990).

[14] H. Ehrenberg, J. A. McAllister, W. G. Marshall, and J. P. Attfield, Compressibility of copper-oxygen bonds: a high-pressure neutron powder diffraction study of CuO, J. Phys.: Condens. Matter **11**, 6501 (1999).

[15] H. Yamada, X.-G. Zheng, Y. Soejima, and M. Kawaminami, Lattice distortion and magnetolattice coupling in CuO, Phys. Rev. B **69**, 104104 (2004).

[16] X. G. Zheng, H. Kubozono, H. Yamada, K. Kato, Y. Ishiwata, and C. N. Xu, Giant negative thermal expansion in magnetic nanocrystals, Nat. Nano **3**, 724 (2008).

[17] P. Blaha, K. Schwarz, G. K. H. Madsen, D. Kvasnicka, J. Luitz, R. Laskowsk, F. Tran, L. Marks, and L. Marks, *WIEN2k: An Augmented Plane Wave Plus Local Orbitals Program for Calculating Crystal Properties* (Techn. Universitat, 2019).

[18] F. Tran, P. Blaha, K. Schwarz, and P. Novák, Hybrid exchange-correlation energy functionals for strongly correlated electrons: Applications to transition-metal monoxides, Phys. Rev. B **74**, 155108 (2006).

[19] B. X. Yang, J. M. Tranquada, and G. Shirane, Neutron scattering studies of the magnetic structure of cupric oxide, Phys. Rev. B **38**, 174 (1988).

[20] H. Xiang, C. Lee, H.-J. Koo, X. Gong, and M.-H. Whangbo, Magnetic properties and energy-mapping analysis, Dalton Trans. **42**, 823 (2012).

[21] G. Radtke, A. Saúl, H. a. Dabkowska, G. M. Luke, and G. a. Botton, Interplay Between Structural, Electronic, and Magnetic Degrees of Freedom in $Sr_3Cr_20_8$, Phys. Rev. Lett. **105**, 036401 (2010).

[22] A. Saúl, D. Vodenicarevic, and G. Radtke, Theoretical study of the magnetic order in α-CoV_2O_6, Phys. Rev. B **87**, 024403 (2013).

[23] A. Saúl and G. Radtke, Density functional approach for the magnetism of β-$TeVO_4$, Phys. Rev. B **89**, 104414 (2014).

[24] M. Okada, H. Tanaka, N. Kurita, K. Johmoto, H. Uekusa, A. Miyake, M. Tokunaga, S. Nishimoto, M. Nakamura, M. Jaime, G. Radtke, and A. Saúl, Quasi-two-dimensional Bose-Einstein condensation of spin triplets in the dimerized quantum magnet $Ba_2CuSi_2O_6Cl_2$, Phys. Rev. B **94**, 094421 (2016).

[25] A. Saúl, N. Gauthier, R. M. Askari, M. Côté, T. Maris, C. Reber, A. Lannes, D. Luneau, M. Nicklas, J. M. Law, E. L. Green, J. Wosnitza, A. D. Bianchi, and A. Feiguin, Unconventional field induced phases in a quantum magnet formed by free radical tetramers, Phys. Rev. B **97**, 064414 (2018).

[26] M. J. Freiser, Thermal variation of the pitch of helical spin configurations, Phys. Rev. **123**, 2003 (1961).

[27] H. Katsura, N. Nagaosa, and A. V. Balatsky, Spin Current and Magnetoelectric Effect in Noncollinear Magnets, Phys. Rev. Lett. **95**, 057205 (2005).

[28] J. W. Loram, K. A. Mirza, C. P. Joyce, and A. J. Osborne, Specific-heat evidence for quasi-1D magnetic order in CuO, EPL **8**, 263 (1989).

[29] A. T. Boothroyd, A. Mukherjee, S. Fulton, T. G. Perring, R. S. Eccleston, H. A. Mook, and B. M. Wanklyn, High-energy magnetic excitations in CuO, Physica B: Condens. Matter **234**, 731 (1997).

[30] T. Shimizu, T. Matsumoto, A. Goto, K. Yoshimura, and K. Kosuge, Spin susceptibility of the quasi-one-dimensional antiferromagnet CuO, Physica B **259–261**, 573 (1999).

[31] T. Shimizu, T. Matsumoto, A. Goto, T. V. Chandrasekhar Rao, K. Yoshimura, and K. Kosuge, Spin susceptibility and superexchange interaction in the antiferromagnet CuO, Phys. Rev. B **68**, 224433 (2003).

[32] C. Yasuda, S. Todo, K. Hukushima, F. Alet, M. Keller, M. Troyer, and H. Takayama, Néel Temperature Of Quasi-Low-Dimensional Heisenberg Antiferromagnets, Phys. Rev. Lett. **94**, 217201 (2005).

[33] J. Mokdad, G. Knebel, C. Marin, J.-P. Brison, I. Matei, and D. Braithwaite, Probing insulators under pressure, Rev. Sci. Instrum. **91**, 093902 (2020).

[34] H. Jacobsen, S. M. Gaw, A. J. Princep, E. Hamilton, S. Tóth, R. A. Ewings, M. Enderle, E. M. H. Wheeler, D. Prabhakaran, and A. T. Boothroyd, Spin dynamics and exchange interactions in CuO measured by neutron scattering, Phys. Rev. B **97**, 144401 (2018).

[35] X. Rocquefelte, M.-H. Whangbo, A. Villesuzanne, S. Jobic, F. Tran, K. Schwarz, and P. Blaha, Short-range magnetic order and temperature-dependent properties of cupric oxide, J. Phys. Condens. Matter **22**, 045502 (2010).

[36] X. Rocquefelte, K. Schwarz, and P. Blaha, Theoretical investigation of the magnetic exchange interactions in copper(II) oxides under chemical and physical pressures, Sci. Rep. **2**, 759 (2012).

[37] See Supplemental Material at http://link.aps.org/supplemental/10.1103/PhysRevB.103.214432 for more details on calculated MCA under hydrostatic pressure up to 38 GPa.

[38] P. J. Brown, T. Chattopadhyay, J. B. Forsyth, and V. Nunez, Antiferromagnetism in CuO studied by neutron polarimetry, J. Phys. Condens. Matter **3**, 4281 (1991).

[39] M. Ain, A. Menelle, B. M. Wanklyn, and E. F. Bertaut, Magnetic structure of CuO by neutron diffraction with polarization analysis, J. Phys. Condens. Matter **4**, 5327 (1992).

[40] D. Dai, H.-J. Koo, and M.-H. Whangbo, Investigation of the incommensurate and commensurate magnetic superstructures of $LiCuVO_4$ and CuO on the basis of the isotropic spin exchange and classical spin approximations, Inorg. Chem. **43**, 4026 (2004).

[41] X. G. Zheng, Y. Sakurai, Y. Okayama, T. Q. Yang, L. Y. Zhang, X. Yao, K. Nonaka, and C. N. Xu, Dielectric measurement to probe electron ordering and electron-spin interaction, J. Appl. Phys. **92**, 2703 (2002).